Published in final edited form as:
Magn Reson Med. 2005 January ; 53(1): 194–200.

Motion-Corrected Free-Breathing Delayed Enhancement Imaging of Myocardial Infarction

Peter Kellman[1,*], **Andrew C. Larson**[2], **Li-Yueh Hsu**[1], **Yiu-Cho Chung**[3], **Orlando P. Simonetti**[3], **Elliot R. McVeigh**[1], and **Andrew E. Arai**[1]

[1]*Laboratory of Cardiac Energetics, National Heart, Lung, and Blood Institute, National Institutes of Health, DHHS, Bethesda, Maryland.* [2]*Departments of Biomedical Engineering and Radiology, Northwestern University, Chicago, Illinois.* [3]*Siemens Medical Solutions, USA, Chicago, Illinois.*

Abstract

Following administration of Gd-DTPA, infarcted myocardium exhibits delayed enhancement and can be imaged using an inversion-recovery sequence. A conventional segmented acquisition requires a number of breath-holds to image the heart. Single-shot phase-sensitive inversion-recovery (PSIR) true-FISP may be combined with parallel imaging using SENSE to achieve high spatial resolution. SNR may be improved by averaging multiple motion-corrected images acquired during free breathing. PSIR techniques have demonstrated a number of benefits including consistent contrast and appearance over a relatively wide range of inversion recovery times (TI), improved contrast-to-noise ratio, and consistent size of the enhanced region. Comparison between images acquired using segmented breath-held turbo-FLASH and averaged, motion-corrected, free-breathing true-FISP show excellent agreement of measured CNR and infarct size. In this study, motion correction was implemented using image registration postprocessing rather than navigator correction of individual frames. Navigator techniques may be incorporated as well. Published 2004 Wiley-Liss, Inc.†

Keywords

MRI; delayed enhancement; heart; myocardial infarction; phase sensitive; SENSE; parallel MRI; free-breathing; motion correction

Myocardial viability assessment using Gd-DTPA enhancement MRI is gaining clinical acceptance (1,2). Using recent MRI methods (3) myocardial infarction (MI) may be imaged with high spatial resolution and good contrast. Following administration of Gd-DTPA, infarcted myocardium exhibits delayed enhancement and can be imaged using an inversion-recovery (IR) sequence (1-3). Using a conventional segmented acquisition requires a number of breath-holds to image the heart.

This paper introduces a method for free-breathing acquisition of delayed enhancement imaging and a quantitative evaluation is presented. Single-shot IR true-FISP may be combined with parallel imaging using SENSE to achieve high spatial resolution (4,5) comparable to conventional segmented IR turbo-FLASH. A single-shot acquisition eliminates the requirement for breath-holding. A phase-sensitive inversion-recovery (PSIR) method (6) combined with parallel imaging reconstruction was used. PSIR techniques have demonstrated a number of benefits including consistent contrast and appearance over a relatively wide range of inversion recovery times (TI), improved contrast-to-noise ratio (CNR), and accurate

*Correspondence to: Peter Kellman, Laboratory of Cardiac Energetics, National Institutes of Health, National Heart, Lung, and Blood Institute, 10 Center Drive, MSC-1061, Building 10, Room B1D416, Bethesda, MD 20892-1061. E-mail: kellman@nih.gov

depiction of the enhanced region. Enhanced signal-to-noise ratio (SNR) may be achieved by averaging multiple motion-corrected images acquired during free breathing. Multiple free-breathing images were motion corrected using a multiscale, subpixel, intensity-based image registration method (7,8). Image registration was constrained to rigid body transformation.

Averaged free-breathing images were compared with images acquired using a standard breath-held segmented IR turbo-FLASH sequence. While true-FISP has a $\sqrt{(T_2/T_1)}$ dependence in steady state, Scheffler and Hennig (9) have shown that inversion recovery with true-FISP readout closely follows the predicted T_1-weighted recovery and is actually more accurate than the standard IR turbo-FLASH. Comparison between the two sequences included measurement of CNR between normal and infarcted tissue and quantitative measurement of MI size using an objective computerized technique.

METHODS

Pulse Sequence

The pulse sequence timing is diagrammed in Fig. 1. For each slice, imaging was performed in mid-diastole using a prospectively gated single-shot acquisition of *k*-space. Inversion recovery pulses were applied every other heartbeat to permit nearly full recovery of magnetization in the presence of Gd-DTPA. This minimizes any disruption of the steady state due to heart rate variability. A reference phase map was acquired at the same cardiac phase in alternate heartbeats using a reduced flip angle readout (6).

A single-shot true-FISP pulse sequence was used (10), whereas the previously described PSIR delayed enhancement sequence (6) was a segmented turbo-FLASH sequence. The inversion was performed via a nonselective, Silver-Hoult adiabatic pulse (11). The T_1-weighted IR image was acquired using multiple 50° flip angle pulses, while the reference used 8° flip angle pulses. The sequence used a run-up ($N = 20$ pulses) with linear ramp flip angle to reduce the transient during steady-state approach (12) for both IR and reference readout acquisitions. The reference image was acquired after the magnetization had recovered almost completely. The use of a 8° flip angle for the reference image reduces the T_1-contrast of the reference image and minimizes effects on the primary T_1-weighted IR image for repeated acquisitions. The inversion recovery of magnetization plotted in Fig. 1 illustrates T_1 values corresponding to normal and contrast enhanced infarcted myocardium. The magnetization of both normal and infarcted myocardium has almost fully recovered after two heartbeats.

Parallel imaging was used for acceleration by a factor of 2 by undersampling the phase encodes acquired for the T_1-weighted IR image. Typically, full resolution corresponded to 128 phase encodes across 300 to 350 mm FOV. The phase encodes acquired for the reference image were fully sampled at a lower (1/2) resolution. The reference phase encodes corresponded to a 2× FOV to prevent any wrap in the reference image.

Image Reconstruction

A phase-sensitive reconstruction method (6) was used that incorporated parallel MR reconstruction for the IR image and B_1-weighted phased array combining for the reference image. A simplified diagram of the reconstruction algorithm is shown in Fig. 2. To improve the SNR of the reference image used for both background phase estimate and surface coil intensity correction, the complex images for each coil were optimally combined (B_1-weighted sum) (6,13) prior to phase-sensitive detection. The complex images for each coil of the IR image were combined using SENSE unmixing coefficients (4), which were computed from the complex reference. The FOV of the reference image was 2× that of the T_1-weighted IR image in order to ensure that there was no aliasing in the reference image used for computing

the SENSE unmixing coefficients; therefore, the spatial resolution of the reference was one fourth that of the IR image. The phase of the reference image was removed from the T_1-weighted IR image on a pixel-by-pixel basis by complex multiplication of the IR image with the conjugate of a reference phase image as shown in Fig. 2 (6). As a result, the real part of the resultant image preserved the polarity of the inversion-recovery signal. The imaginary image was reconstructed as well to ensure that the reference phase was adequate despite potential errors caused by reduced spatial resolution of the reference and by respiratory motion during one heartbeat between IR and reference images. The imaginary image was effectively noise only with no apparent structure in the heart region (results not shown). The surface coil intensity variation was corrected by dividing the IR image with the median filtered reference magnitude image (6). All image reconstruction was performed offline from raw data using Matlab software (The Mathworks, Natick, MA).

Motion Correction

The image registration algorithm (7,8) and C-language source code are open source and freely downloadable (14). The algorithm performs a subpixel registration that minimizes the mean square intensity difference between the two images to be registered. It used an iterative coarse-to-fine pyramid approach to improve speed and convergence. The minimization used a variation of the Marquardt–Levenberg nonlinear least squares optimization. A cubic spline interpolation was used for spatial transformation.

The image registration was performed on a rectangular region that the user interactively selected to encompass the heart across the full range of respiratory motion. The software supported other shaped regions to be defined but a simple bounding box was found to perform well. For short axis image orientation, the bounding box was confined to the left ventricle (LV) in order to avoid including too much of the chest or diaphragm region, which has motion unrelated to the heart; for long axis image orientation the full heart was selected. The motion correction was applied to the full field-of-view images using the transformation parameters calculated from the smaller region.

In-plane motion estimation was constrained to rigid body rotation and translation. The multiscale processing scheme was set at four levels. Motion correction was applied separately to the PSIR images both with and without surface coil intensity correction. Surface coil intensity corrected images have high values in noise-only regions since the reference image used for normalization is essentially noise for these pixels. Registration was performed on the images prior to the surface coil intensity correction and the resulting motion parameters from the least square fit were then applied to the surface coil intensity-corrected images. This scheme was found to be more effective than applying the registration directly to the intensity-corrected images, since adjacent noise-only regions such as the lung maybe within the bounding box and in the case of surface coil intensity correction may contribute higher noise values, which in turn degrades this intensity-based registration method.

For the short axis images where there was little through-plane motion, the target image was simply chosen as the first image in the series of repeated measurements. In the case of long axis images such as the four-chamber view, which had significant through-plane motion, the target was selected to be an image that appeared to be a slice of interest (see Discussion). The registration software output a mean square error (MSE), which served as a goodness of fit. Images with large MSE could be discarded. Motion-corrected images were averaged to enhance SNR. Approximately 30 frames (60 heartbeats) were acquired free-breathing, and various averaging was performed to include: (1) the average of the first 8 frames for direct comparison with the breath held, segmented turbo-FLASH that were acquired in the same 16-heartbeat duration, (2) the best 8 of 30 frames (i.e., frames with least registration error), and (3) the average of all 30 frames.

CNR Comparison

The CNR between MI and normal myocardium was compared for the two methods (segmented turbo-FLASH and single-shot true-FISP) using both simulation and measurement. Simulation was performed by calculating the magnetization of each readout during the inversion recovery according to the methods described by Sekihara (15), using values for T_1 of 245 and 390 msec for MI and normal myocardium, respectively. CNR was measured by subtracting the SNR of MI and adjacent normal myocardium regions. SNR was calculated based on the prescan noise values after proper scaling used by image reconstruction.

Infarct Size Measurement

Infarct size was compared using the two sequences using a semi-automatic computerized method (16) for objective measurement. Infarct size was measured on surface coil intensity-corrected PSIR images for segmented, turbo-FLASH, and single-shot true-FISP, both single frame and first eight averages. The computerized method required the user to draw both endo- and epicardial borders to define the myocardial region of interest. The method then contoured high pixel intensity regions using a threshold value corresponding to half of the maximum intensity after first performing a histogram-based thresholding between normal and infarct pixels. Other image processing steps were included for dealing with microvascular obstructions and reducing false-positive infarct pixels. This method has been validated on in vivo imaging (16).

Experimental Parameters

Delayed enhancement imaging was performed in patients with chronic MI under a clinical research protocol approved by the Institutional Review Board of the National Heart, Lung, and Blood Institute, with prior informed consent. Images are usually acquired between 10 and 30 min after administering a double dose (0.2 mmol/kg) of contrast agent (Gadopentetate Dimeglumine, Berlex Magnevist). Experiments were conducted using a 1.5-T Siemens Sonata MR imaging system. The PSIR turbo-FLASH sequence and reconstruction used Siemens product software. Custom modification to the Siemens product PSIR true-FISP sequence and reconstruction software was made to incorporate parallel imaging using SENSE. A custom eight-element cardiac phased array (Nova Medical, Inc, Wilmington, MA) was used, consisting of two four-element gapped linear arrays (22 cm × 5.25 cm element size with long dimension oriented along the S/I direction and approximately 1.25-cm gap in the L/R direction), with one array positioned on the chest and the second array positioned on the back of the patient. Raw data including prescan noise were acquired for all scans and images were reconstructed off-line.

For each slice imaged, data were acquired for (1) multiple ($N \approx 30$) free-breathing repetitions using the IR-true FISP sequence with rate 2 SENSE acceleration and (2) a breath-held segmented turbo-FLASH acquisition, with both scans acquired close in time (within 60 sec). For several subjects the turbo-FLASH acquisitions were made both before and after the IR-true FISP to ensure that there was no acquisition order dependence. For both methods, the same FOV, spatial resolution, and TI were used. With the parameters used, IR-turboFLASH required a 16-heartbeat breath-hold per slice, whereas the PSIR true-FISP required a 2-heartbeat acquisition (per repetition). Imaging was performed in diastasis with approximately the same acquisition window for both methods. Typical parameters for the IR-true-FISP sequence were BW 977 Hz/pixel, TE/TR 1.2/2.7 msec, 50° readout flip angle (8° reference), 256 × 128 image matrix, with FOV varying between 300 and 370 mm. Parallel imaging was used to reduce the imaging duration by acquiring 64 phase encodes in a single heartbeat (172-msec window) with 2 R–R intervals between inversions and reconstructing to obtain the full 128-line image resolution using rate $R = 2$ SENSE. A trigger delay was used to position the acquisition in mid-diastole. The value of the trigger delay depends on the heart rate and IR prep time (TI). Typical

value for the trigger delay is in the range 300–400 msec. Typical parameters for the IR-turbo-FLASH sequence were BW 140 Hz/pixel, TE/TR 3.9/8.5 msec, 30° readout flip angle (5° reference), 256 × 136 image matrix. The phase-encode dimension was slightly oversampled, due to the manner in which the sequence treats segmented acquisition, yielding an effective resolution of 128 lines in this specific example. The 136 phase encodes were acquired in 16 heartbeats collecting 17 lines per heartbeat with 2 R–R intervals between inversions. The segment duration was 145 msec per R–R interval, acquired during diastasis. The parameters used for the IR-turboFLASH are similar to those used in practice at a number of sites (17).

Short axis slices were acquired in $n = 6$ patients with chronic MI and long axis images were acquired in 2 of the patients. The mean age of the patients was 53.2 ± 10.7 years (mean ± STD). The mean weight of the patients was 202 ± 27 lb (mean ± STD). The mean heart rate of the patients was 61.5 ± 10.3 bpm (mean ± STD). All patients were male. In addition to free-breathing acquisitions, several breath-held acquisitions were made using the proposed single shot true-FISP method to examine the degree of stability during a breath hold.

RESULTS

Short-axis images of the heart for a patient with inferior and inferolateral MI and a smaller anterolateral MI are shown in Fig. 3 comparing (a) the “standard” breath-held, segmented IR-turboFLASH, (b) a single free-breathing, single-shot IR-trueFISP image, (c) average of the first 8 repetitions free-breathing with motion correction, (d) average of the best 8 of 29 repetitions free-breathing with motion correction, and (e) average of all 29 repetitions free-breathing with motion correction. The acquisition time was the same (16 heartbeats) for cases in Fig. 3a and c) In this example, the spatial resolution was $1.4 \times 2.7 \times 6\text{mm}^3$ with FOV $350 \times 350\ \text{mm}^2$ and TI = 300 msec. The smaller anterolateral MI, which is difficult to detect without averaging (Fig. 3b), is readily discernible after averaging with motion correction (Fig. 3c-e). Short-axis images for a second patient with anterolateral MI are shown in Fig. 4 as another example.

The motion parameters and mean square error (arbitrary units) of the registration are plotted in Fig. 5a for the first patient shown in Fig. 3, where each time image frame is spaced by 2 heartbeats at approximately 73 bpm. The oscillatory characteristic is due to sampling at close to two images (4 heartbeats) per respiratory cycle. The error and fit parameters are plotted in Fig. 5b after sorting based on mean square error. The average in Fig. 3d is composed of the first 8 frames after sorting, i.e., 8 with minimum error. The mean in-plane translation for the 6 patients was 3.1 ± 1.6 pixels, and the maximum translation ranged from 3.5 to 15 pixels. The maximum in-plane rotation ranged from 1.1 to 11.5°.

Motion-corrected averaging was applied to long-axis images acquired during free breathing. In the case of long axis imaging there is substantial through-plane motion and the slice with MI is not in every frame due to respiratory motion. Figure 6a shows and average of the best 8 frames (i.e., with lowest registration error) using frame 2, which contains the MI as the target for registration; the sorted error for this case is plotted in Fig. 6b. Figure 6c shows and average of the best 8 frames using frame 13 (a slice without MI) as the target for registration; the sorted error for this case is plotted in Fig. 6d. The respiratory phase corresponding to Fig. 6c is close to end-expiration; thus, there are a greater number of frames that fit closely as seen by plot of error in Fig. 6d. The desired slice with MI was not optimally acquired at end-expiration and, therefore, the averaging was limited.

The magnetization during inversion recovery for the two sequences was simulated to compare the CNR between MI and normal myocardium. The difference in magnetization $\Delta M/M_0$ is approximately 1.4:1 greater for the true-FISP readout as seen in Fig. 7; however, the SNR loss

due to greater bandwidth used by true-FISP was 2.6:1. Note that the plot in Fig. 7a has a staircase appearance due to the segmented acquisition with interleaved phase encode order. The CNR for the segmented turbo-FLASH method is predicted to be approximately 2.7 times that of the true-FISP with SENSE for a single frame without averaging using the specific imaging parameters used after accounting for acceleration loss and SENSE *g*-factor. The maximum value of the SENSE *g*-factor for rate 2 acceleration using the custom eight-element linear array is typically 1.05 in the heart region. The CNR for the image with 8 averages is improved by $\sqrt{8} \approx 2.8$, yielding approximately the same CNR as the breath-held turbo-FLASH acquired in the same time. The calculations for the CNR comparison are described by Eq [1].

$$\frac{\mathrm{CNR}_{\mathrm{FLASH}}}{\mathrm{CNR}_{\mathrm{FISP}}} = \frac{\left(\Delta M / M_0\right)_{\mathrm{FLASH}}}{\left(\Delta M / M_0\right)_{\mathrm{FISP}}} \frac{\left(\sqrt{N_{\mathrm{PE}} / \mathrm{BW}}\right)_{\mathrm{FLASH}}}{\left(\sqrt{N_{\mathrm{PE}} / \mathrm{BW}}\right)_{\mathrm{FISP}}} \frac{1}{\left(1 / g_{\mathrm{SENSE}}\right)} \frac{\left(\sqrt{N_{\mathrm{avg}}}\right)_{\mathrm{FLASH}}}{\left(\sqrt{N_{\mathrm{avg}}}\right)_{\mathrm{FISP}}} \quad [1]$$

$$= \frac{0.08}{0.11} \frac{\sqrt{136 / 140}}{\sqrt{64 / 977}} \frac{1}{\sqrt{1 / 1.05}} \frac{1}{\sqrt{8}} \approx 1.04.$$

The measured CNR for free-breathing motion corrected IR-true FISP with 8 averages was 0.96 ± 0.13 (mean ± SD, $n = 6$) times that for breath-held IR-turbo-FLASH, which is in close agreement with prediction. Averaging was extended for 30 images acquired in 60 heartbeats to further increase CNR (approximately double that of the IR-turbo-FLASH case) with minimal motion blurring or loss of detail after registration (see Fig. 3e).

The comparison of infarct size measurements is shown in Fig. 8, which plots the size for the single-shot true-FISP sequence versus the breath-held, segmented turbo-FLASH. The bold-line corresponds to the average of first 8 frames after motion correction, and the lighter line is for the first frame without averaging. The infarct size for averaged images is in close agreement with the turbo-FLASH method ($R^2 = 0.98$) over a wide range of MI sizes, while the single frame data are more scattered ($R^2 = 0.87$), as expected.

DISCUSSION

The incorporation of parallel imaging and image registration-based motion correction has enabled the single-shot method to achieve comparable image quality in the same duration image acquisition. In other words, the CNR between MI and normal myocardium was approximately the same for the segmented, breath-held turbo-FLASH and free-breathing, single-shot true-FISP with eight averages, with the same spatial resolution, both acquired in 16 heartbeats. This result is in excellent agreement between the comparison of measured CNR and that predicted by simulation. There was also close agreement between quantitative measurement of infarct size using an objective computerized method.

Multiple frames were also acquired using the single-shot true-FISP method with eight frames (16 heartbeat) during a breath hold. Surprisingly, there was significant respiratory motion apparent in the course of the breath hold, with the heart motion on the order of 1 pixel in several cases. This respiratory motion resembled a slow linear drift. This type of motion is also present in segmented acquisitions and may slightly degrade the spatial resolution.

Prior study (18) of single-shot FISP delayed enhancement imaging reported lower detection sensivity for smaller MI. However, that study used a lower spatial resolution and did not perform averaging for SNR enhancement.

Through-plane motion was not observed to be a problem for short-axis imaging orientation but was significant for the long-axis orientation, particularly the four-chamber view. By discarding

images with larger registration errors, the through-plane motion was largely mitigated at the expense of reduced averaging efficiency. This is akin to using retrospective respiratory gating. By incorporating navigator approaches for slice following, it may be possible to sufficiently minimize the through-plane motion and restore the averaging efficiency in these cases. In the example of Fig. 3c, which averaged the best eight frames, the first frame was used as the target. The shape of the sorted error curve (Fig. 5b), which dictates the averaging efficiency, depends on which frame is selected as a target (i.e., respiratory phase). In other words, if the target frame is near end expiration, there are likely to be more frames at the same respiratory phase. It may be possible to find an efficient way to select the optimum target frame without resorting to brute force testing of all frames. For short-axis imaging, there was negligible motion with the specified imaging parameters.

Using the intensity based-image registration (7) required the selection of a bounding region for motion estimation. A simple rectangular bounding box was used and found to be effective in all cases. The bounding region was selected to encompass the LV over full range of respiratory motion, but was otherwise minimized to exclude other regions that might have different motion. There are numerous image registration methods (19,20) that might also be appropriate for delayed enhancement imaging and should be evaluated.

CONCLUSION

In the same imaging time as required for a conventional breath-held segmented imaging approach, the new free-breathing method achieves approximately the same spatial resolution and CNR. Using SENSE acceleration, it is possible to use single-shot true-FISP without compromising spatial resolution. Multiple images may be registered and averaged to enhance SNR without discernible motion blurring. This approach overcomes the prior limitation of single-shot FISP in detecting smaller infarcts (18). The smaller anterolateral MI, which is difficult to detect without averaging (Fig. 3b), is readily discernible after averaging with motion correction (Fig. 3c-e).

This method is particularly attractive in cases where patients have difficulty holding their breath. Improved CNR through extended averaging will improve discimination between LV blood pool and subendocardial MI and will also be important at lower contrast doses, reduced slice thickness, or improved in-plane resolution. In the case of long-axis image orientations, which have substantial through-plane motion, the averaging method has been modified to automatically discard frames that have large registration error in a similar fashion as retrospective respiratory gating. Preliminary experience with long-axis orientation has used approximately 25–30% of the frames. This method may be modified to incorporate navigators for slice following to improve the acquisition efficiency. Further improvement in SNR may be achieved by averaging an increased number of frames (beyond the limit of breath holding).

REFERENCES

1. Kim RJ, Fieno DS, Parrish TB, Harris K, Chen EL, Simonetti O, Bundy J, Finn JP, Klocke FJ, Judd RM. Relationship of MRI delayed contrast enhancement to irreversible injury, infarct age, and contractile function. Circulation 1999;100:1992–2002. [PubMed: 10556226]
2. Kim RJ, Wu E, Rafael A, Chen EL, Parker MA, Simonetti O, Klocke FJ, Bonow RO, Judd RM. The use of contrast-enhanced magnetic resonance imaging to identify reversible myocardial dysfunction. N Engl J Med 2000;343:1445–1453. [PubMed: 11078769]
3. Simonetti OP, Kim RJ, Fieno DS, Hillenbrand HB, Wu E, Bundy JM, Finn JP, Judd RM. An improved MR imaging technique for the visualization of myocardial infarction. Radiology 2001;218:215–223. [PubMed: 11152805]
4. Pruessmann KP, Weiger M, Scheidegger MB, Boesiger P. SENSE: sensitivity encoding for fast MRI. Magn Reson Med 1999;42:952–962. [PubMed: 10542355]

5. Kellman P, Larson AC, Chung Y, Simonetti OP, McVeigh ER, Arai AE. Multi-slice delayed hyperenhancement imaging of myocardial infarction using SENSE accelerated phase sensitive inversion recovery true-FISP. J Cardiovasc Magn Reson 2004;6:162–163.
6. Kellman P, Arai AE, McVeigh ER, Aletras AH. Phase sensitive inversion recovery for detecting myocardial infarction using gadolinium delayed hyperenhancement. Magn Reson Med 2002;47:372–383. [PubMed: 11810682]
7. Thevenaz P, Unser M. A pyramid approach to subpixel registration based on intensity. IEEE Trans Image Proc 1998;7:27–41.
8. Thevenaz P, Ruttimann UE, Unser M. Iterative multi-scale registration without landmarks. Proc IEEE Intl Conf Image Proc 1995;3:228–231.
9. Scheffler K, Hennig J. T1 quantification with inversion recovery true-FISP. Magn Reson Med 2002;45:620–623.
10. Chung YC, Vargas J, Simonetti OP, Kim R, Judd R. Infarct imaging in a single heart beat. J Cardiovasc Magn Reson 2002;4:12–13.
11. Silver MS, Joseph RI, Hoult DI. Highly selective PI/2 and PI-pulse generation. J Magn Reson 1984;59:347–351.
12. Deshpande VS, Chung YC, Zhang Q, Shea SM, Li D. Reduction of transient signal oscillations in true-FISP using a linear flip angle series magnetization preparation. Magn Reson Med 2003;49:151–157. [PubMed: 12509831]
13. Roemer PB, Edelstein WA, Hayes CE, Souza SP, Mueller OM. The NMR phased array. Magn Reson Med 1990;16:192–225. [PubMed: 2266841]
14. http://bigwww.epfl.ch/thevenaz/registration/index.html
15. Sekihara K. Steady-state magnetizations in rapid NMR imaging using small flip angles and short repetition intervals. IEEE Trans Med Imaging 1987;6:157–164.
16. Hsu, L.; Kellman, P.; Natanson, A.; Aletras, AH.; Arai, AE. Computer quantification of myocardial infarction on contrast enhanced magnetic resonance imaging; Proceedings of the 12th Annual Meeting of ISMRM; Kyoto, Japan. 2004. p. 171
17. Kim RJ, Shah DJ, Judd RM. How we perform delayed enhancement imaging. J Cardiovasc Magn Reson 2003;5:505–514. [PubMed: 12882082] Erratum in J Cardiovasc Magn Reson 2003;5:613–615.
18. Lee DC, Wu E, Chung YC, Simonetti OP, Elliot M, Holly TA, Klocke FJ, Bonow RO. Comparison between single shot trueFISP and segmented turboFLASH for the detection of myocardial infarction. J Cardiovasc Magn Reson 2003;5:79–80.
19. Maintz JB, Viergever MA. A survey of medical image registration. Med Image Anal 1998;2:1–36. [PubMed: 10638851]
20. Hill DL, Batchelor PG, Holden M, Hawkes DJ. Medical image registration. Phys Med Biol 2001;46:R1–R45. [PubMed: 11277237]

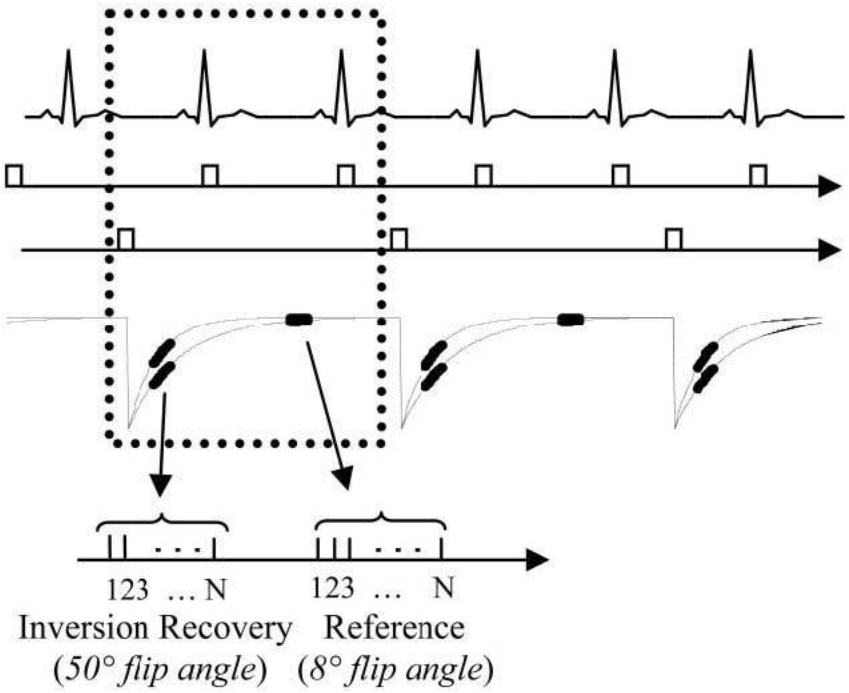

FIG 1.
Pulse sequence diagram for single-shot inversion recovery true-FISP with acquisition of IR and reference images for PSIR image reconstruction. Data for IR and reference images are collected alternately every other heartbeat.

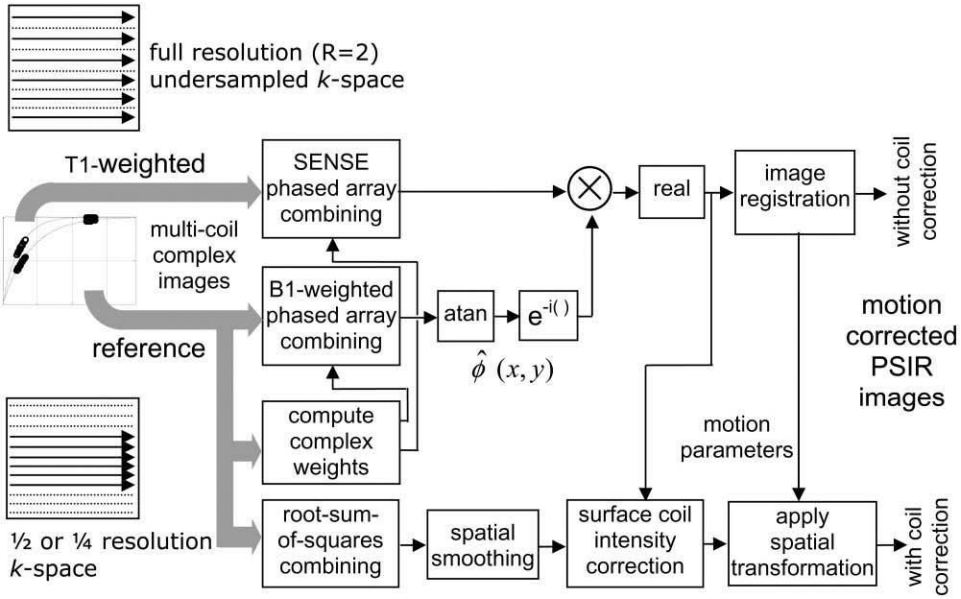

FIG 2.

Image reconstruction (simplified diagram) for parallel imaging with phase-sensitive inversion recovery, surface coil intensity correction, and motion correction.

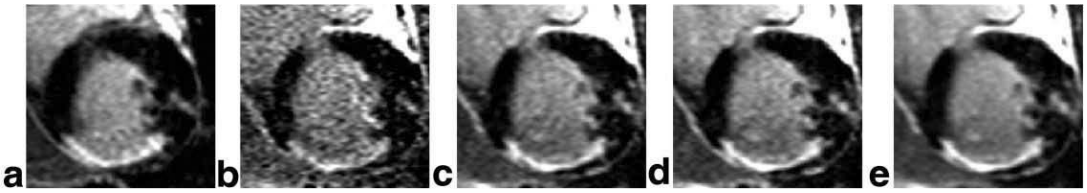

FIG 3.

Short-axis images of the heart for a patient with inferior and inferolateral MI and a smaller anterolateral MI comparing (**a**) the "standard" breath-held, segmented IR-turbo-FLASH, (**b**) a single free-breathing, single shot IR-true-FISP image, (**c**) average of the first 8 repetitions free-breathing with motion correction, (**d**) average of the best 8 of 29 repetitions free-breathing with motion correction, and (**e**) average of all 29 repetitions free-breathing with motion correction.

FIG 4.

Short-axis images of the heart for a second patient with anteroseptal MI comparing (**a**) the "standard" breath-held, segmented IR-turbo-FLASH, (**b**) a single free-breathing, single shot IR-true-FISP image, (**c**) average of the first 8 repetitions free-breathing with motion correction, (**d**) average of the best 8 of 30 repetitions free-breathing with motion correction, and (**e**) average of all 30 repetitions free-breathing with motion correction.

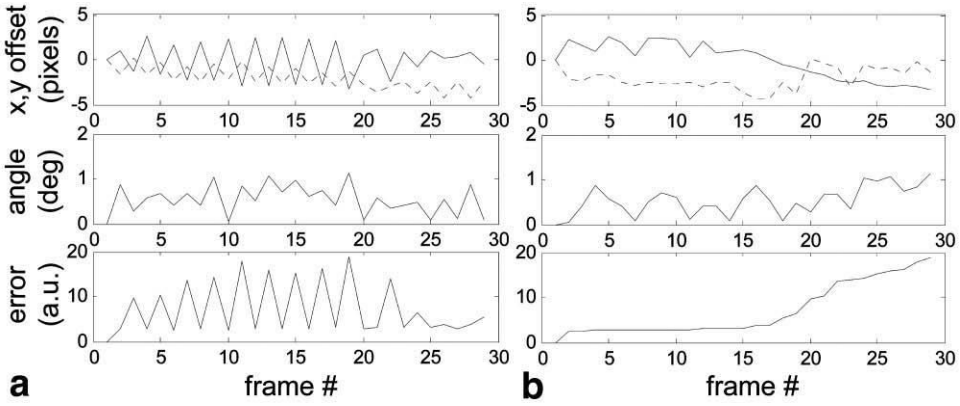

FIG 5.

Motion parameters and mean square registration error (arbitrary units) (**a**) versus acquired frame number and (**b**) sorted based on mean square error.

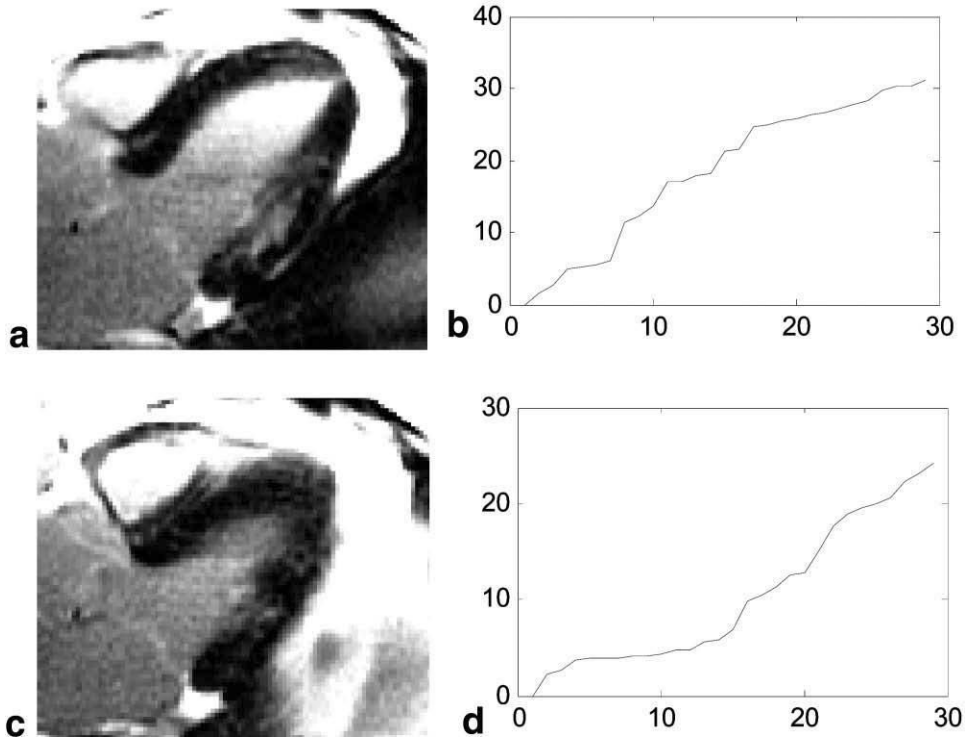

FIG 6.

Motion-corrected averages of long-axis images acquired during free breathing illustrating significant through-plane motion. The images shown represent averages of images selected from two different respiratory phases: (**a**) a slice which contains the MI and (**c**) a slice where respiratory motion has moved the MI out of the imaging plane. (a) and (c) are calculated as the average of the 8 frames with lowest registration error using two different target frames for registration, respectively. The sorted registration error shown in (**b**) and (**d**) corresponds to (a) and (c), respectively.

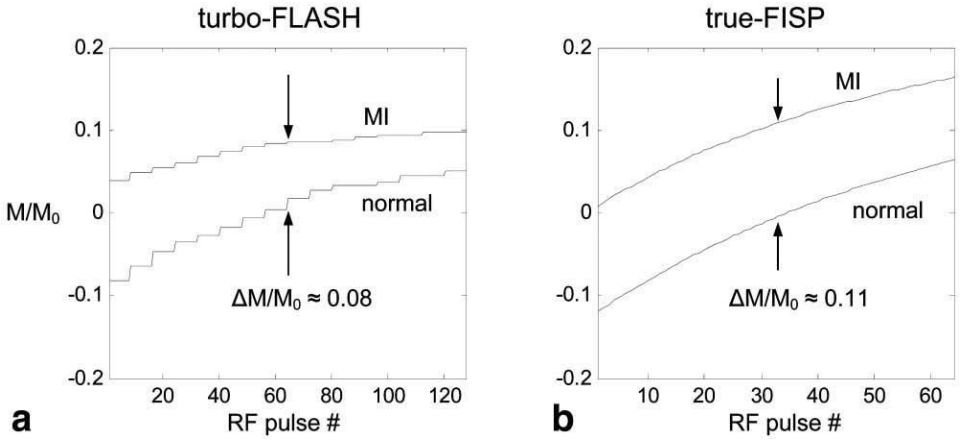

FIG 7.

Magnetization during inversion recovery for MI and normal myocardium and specified imaging parameters for (**a**) segmented turbo-FLASH and (**b**) single-shot true-FISP with $R = 2$ SENSE acceleration.

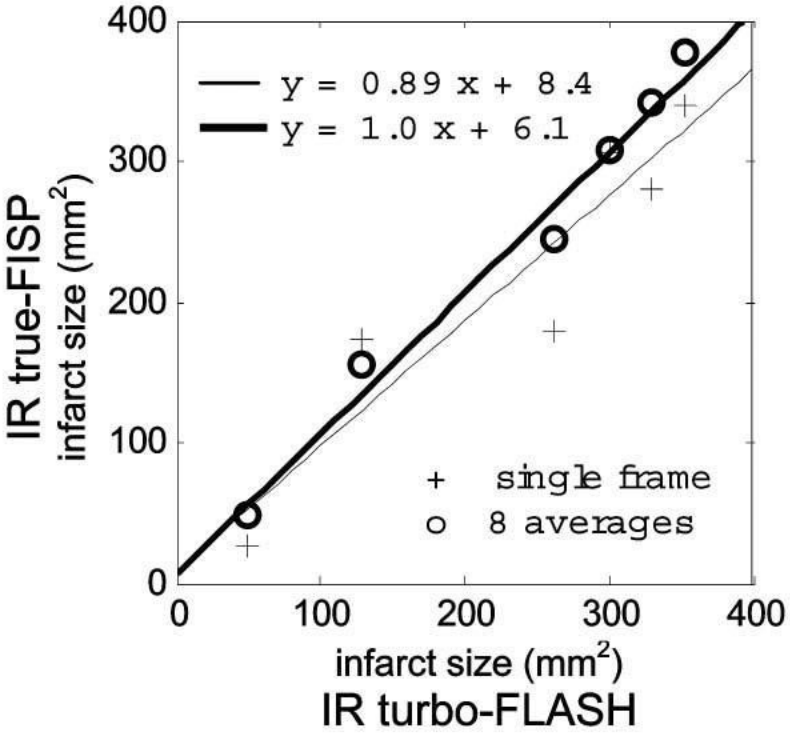

FIG 8.

Comparison of infarct size measured in the breath-held, segmented turbo-FLASH images with motion corrected, free-breathing, single-shot, true-FISP images. The bold line and circles show results from averaging eight true-FISP images; the thin line and crosses show results from one single-shot true-FISP image.